The Astrophysical Journal, 835:127 (11pp), 2017 February 1 doi:10.3847/1538-4357/835/2/127
© 2017. The American Astronomical Society. All rights reserved.

What Lurks in ULIRGs?—Probing the Chemistry and Excitation of Molecular Gas in the Nuclei of Arp 220 and NGC 6240

Swarnima Manohar and Nick Scoville
California Institute of Technology, MC 249-17, 1200 East California Boulevard, Pasadena, CA 91125, USA
Received 2016 February 23; revised 2016 November 25; accepted 2016 December 7; published 2017 January 23

Abstract

We have imaged the dense star-forming regions of Arp 220 and NGC 6240 in the 3 mm band transitions of CO, HCN, HCO^+, HNC, and CS at 0.″5–0.″8 resolution using CARMA. Our data set images all these lines at similar resolutions and high sensitivity, and can be used to derive line ratios of faint high excitation lines. In both the nuclei of Arp 220, the HCN/HNC ratios suggest chemistry of X-ray Dominated Regions (XDRs)—a likely signature of an active galactic nucleus. In NGC 6240, there is no evidence of XDR type chemistry, but there the bulk of the molecular gas is concentrated between the nuclei rather than on them. We calculated molecular H_2 densities from excitation analysis of each of the molecular species. It appears that the abundances of HNC and HCO^+ in Ultra Luminous Infrared Galaxies may be significantly different from those in galactic molecular clouds. The derived H_2 volume densities are $\sim 5 \times 10^4$ cm^{-3} in the Arp 220 nuclei and $\sim 10^4$ cm^{-3} in NGC 6240.

Key words: galaxies: individual (Arp 220 and NGC 6240) – galaxies: starburst

1. Introduction

Galactic merging is a key step in the evolution and buildup of galaxies in the universe. It is also strongly correlated with the most luminous active galactic nucleus (AGN) activity and high star formation rates (SFRs). Ultra Luminous Infra-Red Galaxies (ULIRGs) emit as much as 90% of their luminosity in the infrared ($L_{\rm IR} > 10^{12}\,L_\odot$). Evidence of ongoing or recent mergers in a substantial fraction of these objects suggests that the merger process is an essential trigger for these energetic and active galaxies (Sanders et al. 1988; Veilleux et al. 2002).

NGC 6240 ($L_{\rm IR} \sim 10^{11.9}\,L_\odot$) and Arp 220 ($L_{\rm IR} \sim 2 \times 10^{12}\,L_\odot$) are often viewed as prototypical ULIRGs, albeit at slightly different stages of merging. They show high SFRs, ∼100 and 240 $M_\odot$ yr^{-1} respectively, estimated from IR luminosity (Anantharamaiah et al. 2000; Beswick et al. 2001; Sanders et al. 2003). NGC 6240 exhibits two clearly separated nuclei ∼2″ (∼1 kpc, Tacconi et al. 1999) apart, both showing a hard X-ray source AGN (Komossa et al. 2003). However, the major gas concentration lies between the two nuclei in the overlap region (Tacconi et al. 1999; Scoville et al. 2000; Engel et al. 2010).

Near infrared imaging of Arp 220 reveals two nuclei separated by 1″ (projected distance of 370 pc) and one of these has recently been detected in X-rays (Iwasawa et al. 2005). Previous CO imaging at 0.″5 resolution detected counter-rotating disks in both nuclei with radii ∼100 pc, and dynamical masses of $2 \times 10^9\,M_\odot$ in each (Scoville et al. 1997; Sakamoto et al. 1999; Downes & Eckart 2007). Observations by Clements et al. (2002) and McDowell et al. (2003) using *Chandra* can neither confirm nor rule out the presence of AGNs. The inferred visible extinctions perpendicular to the counter-rotating disks, $A_V \sim$ 500–2000 mag, have made direct observation and measurement of physical conditions of the cores of the Arp 220 disks difficult. In particular, the physical conditions of the molecular gas in the nuclei of Arp 220 and in the gas disk of NGC 6240 are poorly determined.

In this paper, we present CARMA molecular line observations of Arp 220 and NGC 6240 at ∼2″ and 0.″6 resolutions. We observed the HCN(1-0), CS(2-1), HNC(1-0), and HCO^+(1-0) transitions, and also the isotopomer lines $H^{13}CN$(1-0) and ^{13}CS(2-1) simultaneously, at similar resolutions and with consistent calibrations. CO(1-0) and ^{13}CO(1-0) transitions were also observed for each of the galaxies at 2″ resolution. These two lines were also observed at 0.″6 resolution for Arp 220. Multi-band imaging has allowed excitation analysis of HCN, HCO^+, HNC, and CS along with CO transitions to constrain the properties of the gas. Our unique data set of high sensitivity observations of different lines at similar resolutions enables the derivation of line ratios of faint high excitation lines.

In this work we are using various molecular species as tracers of the densest H_2, which will also probe the varied chemical and physical processes that are in effect. While CO will map H_2 in general, hydrogen cyanide (HCN) will map gas with ∼100 times higher density. Hydrogen isocyanide (HNC) is expected to probe molecular gas with similar densities to HCN but with different physical processes at play (Goldsmith et al. 1981; Hirota et al. 1998; Pérez-Beaupuits et al. 2007). HCN and HNC can be used to probe the presence of an obscured AGN. Carbon monosulfide (CS) traces high excitation molecular gas (Bayet et al. 2009) while HCO^+, some studies (Graciá-Carpio et al. 2006) indicate, might trace dense gas in starburst driven winds. Isotopomers like $H^{13}CN$ and ^{13}CO trace densities and temperatures of the most optically thick regions (Aalto et al. 1995). Though it is convention to assume that these molecular species (HCN, HNC, HCO^+) map the same component of the molecular gas because of their similar critical densities, it should be pointed out here that, at these spatial resolutions, this may not be true because of their dissimilar chemical and physical properties.

In Section 2, we discuss the details of the observations of Arp 220 and NGC 6240 using CARMA at both 2″ and 0.″5–0.″8 resolution. Section 3 describes the measurements and results from these observations for both systems and compares these with previous measurements. In Section 4, we analyze the physical conditions of the molecular gas based on our

observations and measurements. Section 5 summarizes our analysis and results.

2. Observations

The Combined Array for Research in Millimeter-wave Astronomy (CARMA) was used to observe CO(1-0), HCN(1-0), CS(2-1), HNC(1-0), and HCO^+(1-0) transitions along with isotopomer lines ^{13}CO(1-0), H^{13}CN(1-0), and ^{13}CS(2-1) in Arp 220 and NGC 6240. Observations in the C configuration used antenna separations between 26 and 370 m and led to a resolution of $\sim$1.″7–2″. In the B configuration, the antennas were spaced more widely at 100–1000 m and achieved a higher resolution of $\sim$0.″5–0.″8. The C configuration observations were carried out in good ($\tau_{112\,\mathrm{GHz}} < 0.3$) to fair ($0.5 < \tau_{112\,\mathrm{GHz}} < 0.3$) weather conditions during several runs between 2012 December and 2013 November. The B configuration observations were made between 2013 January and 2014 January and were of similarly high quality.

The spectrometer bands were positioned independently within the IF bandwidth to simultaneously observe the HCN (1-0), CS(2-1), HNC(1-0), and HCO^+(1-0) lines along with isotopomer lines H^{13}CN(1-0) and ^{13}CS(2-1) in both Arp 220 and NGC 6240. The correlator was configured to have eight 500 MHz bands in the lower and upper sidebands with 95-channel spectral resolution per band. Each band corresponds to $\sim$1500 km s^{-1} in velocity space. Each channel corresponds to 5.208 MHz width, $\sim$15 km s^{-1}. CO(1-0) and ^{13}CO(1-0) were observed in a separate correlator configuration. The data were reduced using the MIRIAD (Multichannel Image Reconstruction, Image Analysis and Display) package. Subsequent analysis, involving for example line profiles and intensity measurements, used MATLAB.

Total observation time for Arp 220, in C configuration, for observations of HCN(1-0), CS(2-1), HNC(1-0), HCO^+(1-0), H^{13}CN(1-0), and ^{13}CS(2-1) lines was 48.5 hr. In the case of NGC 6240, the observation time was 36.7 hr. Observing times for CO(1-0) and ^{13}CO(1-0) were 16.5 hr and 16.4 hr respectively for Arp 220 and NGC 6240. In the B configuration, the total observation time for Arp 220 for observations of HCN(1-0), CS(2-1), HNC(1-0), HCO^+(1-0), H^{13}CN(1-0), and ^{13}CS(2-1) lines was 49 hr and for NGC 6240, 43.9 hr. For Arp 220, CO(1-0) and ^{13}CO(1-0) were observed for 34.4 hr. Bad weather prevented these lines from being observed for NGC 6240 in the B configuration.

3. Results

Our observations are the first comprehensive, high resolution, interferometric measurements of lower transition lines of high dipole moment molecules like HCN for these galaxies. To compare the lines in both galaxies with each other and with earlier studies, we calculated velocity integrated fluxes and luminosities for observations at both 2″ and 0.″6 resolutions using Solomon et al. (1992b). The results, along with measurements from earlier studies, are presented in Table 1.

Figures 1 and 3 show the spectra of the high density gas tracers for Arp 220 and NGC 6240 respectively at 2″ resolution. The high resolution interferometric observations of CO(1-0) for both the galaxies are in Figure 2. Figure 4 shows the integrated line intensity images for HCN(1-0) emission at 0.″6 resolution for Arp 220 and NGC 6240. The beam size is in blue in the lower right corner. The two nuclei of Arp 220 are clearly seen in this image. The western nucleus is more clearly seen because of stronger emission from it.

In the case of Arp 220, the double peaked profile expected from the counter-rotating molecular gas disks observed in earlier studies (Scoville et al. 1997; Downes & Solomon 1998; Greve et al. 2009) is seen in our CO(1-0) observations. HCN(1-0), CS(2-1), HNC(1-0), and HCO^+(1-0) display a similar double peaked profile. The peaks are stronger and more clearly distinguishable in these lines than in CO. ^{13}CO(1-0) is not clearly a double peaked profile, but seems more square. This suggests that the ^{13}CO(1-0) flux may originate largely from the blueshifted western nucleus of Arp 220. The difference in the CO(1-0) and ^{13}CO(1-0) profiles indicates differences in either the dynamics of the molecular gas or its optical depth in the two nuclei. In this case, it seems most likely that the profile shape difference is probably due to the ^{13}CO(1-0) optical depth being higher in the western nuclei. We were able to detect H^{13}CN(1-0) (Figure 1(f)) at more than the 4σ level; ^{13}CS(2-1) was not detected.

All the lines detected in NGC 6240 show a Gaussian-like velocity profile, in contrast to Arp 220. This suggests that turbulence or disordered random motions, rather than rotation, is dominating the line profiles in NGC 6240 and is consistent with the molecular and dust continuum emission being concentrated between the two stellar nuclei (Scoville et al. 2015), rather than centered on each of the stellar nuclei as in Arp 220. This seems to be the case on a wide range of spatial scales. This is not the case in Arp 220, where the double peak features evolve with the different transition lines that reflect different densities and temperatures (Greve et al. 2009). Isotopomer lines were not detected at any significant level in NGC 6240.

Our observations of CO(1-0), for both Arp 220 and NGC 6240, agree with many previous measurements, for example (Scoville et al. 1997; Downes & Solomon 1998; Bryant & Scoville 1999), giving confidence in our data, methodology and calibrations. However, there are significant discrepancies between our measurements of HCO^+(1-0) flux densities and those from previous studies, especially in comparison with single dish observations. Our fluxes are as much as twice those reported by Solomon et al. (1992a), Graciá-Carpio et al. (2006), and Nakanishi et al. (2005) for both the galaxies (see Table 1).

Our measurement of HCN flux also agrees with interferometric fluxes measured in other studies (Radford et al. 1991; Krips et al. 2008). We have used the same correlator configuration to observe HCN (1-0), HNC (1-0), HCO^+(1-0), and CS (2-1) simultaneously. These observations used the same calibrators, have the same UV coverage and similar synthesized beam sizes (see Table 1). The strong agreement of HCN flux with other interferometric measurements confirms our calibration and methodology. The discrepancy in our measurement of fluxes of HCO^+(1-0) and those done in other studies may be due to errors in calibration in those studies or other methodology differences.

In the following sections we are concentrating on line ratios. Since these flux measurements were made using same calibrators at the same time, with the same UV coverage and similar synthesized beam sizes, any atmospheric errors will be the same for both lines and therefore cancel out.

Table 1
Molecular Transition Lines Detected: Arp 220 and NGC 6240

Line	ARP 220						NGC 6240					
	FWHM (km s^{-1})	HPBW (arcsec)	$S_\nu\Delta v$ (Jy km s^{-1})	L'^c ($\times 10^9$ K km s^{-1} pc^2)	Telescope	References	FWHM (km s^{-1})	HPBW (arcsec)	$S_\nu\Delta v$ (Jy km s^{-1})	L'^c ($\times 10^9$ K km s^{-1} pc^2)	Telescope	References
CO(1-0)	504	2	410 ± 41	5.9 ± 0.6	OVRO	Scoville et al. (1997)	370	...	314 ± 64	8.3 ± 1.7	IRAM 30 m	Solomon et al. (1997)
	...	1.9 × 2.1	384 ± 115	5.5 ± 1.7	OVRO	Scoville et al. (1991)	469	3.3 × 2.4	324 ± 33	8.6 ± 0.9	OVRO	Bryant & Scoville (1999)
	480	...	496 ± 99	7.2 ± 1.4	IRAM 30 m	Solomon et al. (1997)	...	...	322 ± 29	8.5 ± 0.8		
	500	1.6 × 0.9	385 ± 40	6.1 ± 0.64	CARMA	2″, This Work	400	1.9 × 1.0	304 ± 30	8.9 ± 0.88	CARMA	2″, This Work
	450	0.5 × 0.4	350 ± 35	5.2 ± 0.52	CARMA	0.″8, This Work	...	...	...	...	...	...
HCN(1- 0)	...	4.1 × 2.2	35 ± 11	0.85 ± 0.27	IRAM PdBI	Radford et al. (1991)	...	...	26 ± 8	1.17 ± 0.36	IRAM 30 m	Solomon et al. (1992a)
	550	28.3	59 ± 12	1.44 ± 0.29	IRAM 30 m	Greve et al. (2009)	340	28.3	13 ± 3	0.58 ± 0.13	IRAM 30 m	Greve et al. (2009)
	530	...	48 ± 14	1.17 ± 0.34	IRAM 30 m	Krips et al. (2008)	...	2.0 × 1.7	14 ± 4	0.63 ± 0.18	NMA	Nakanishi et al. (2005)
	565	2.0 × 1.2	42 ± 4	1.1 ± 0.11	CARMA	2″, This Work	350	2.2 × 1.3	26 ± 2.6	1.3 ± 0.13	CARMA	2″, This Work
	550	0.7 × 0.5	49 ± 5	1.3 ± 0.13	CARMA	0.″8, This Work	325	0.7 × 0.6	24 ± 2.4	1.2 ± 0.12	CARMA	0.″8, This Work
CS(2-1)	339	25.1	12 ± 3	0.24 ± 0.06	IRAM 30 m	Greve et al. (2009)	...	26	7.5 ± 1.5	0.3 ± 0.06	Herschel	Papadopoulos et al. (2014)
	345	1.7 × 1.1	11 ± 0.1	0.24 ± 0.02	CARMA	2″, This Work	175	1.9 × 1.2	3 ± 0.6	0.12 ± 0.02	CARMA	2″, This Work
	375	0.6 × 0.5	17 ± 2	0.38 ± 0.04	CARMA	0.″8, This Work	200	0.6 × 0.5	12 ± 1	0.05 ± 0.01	CARMA	0.″8, This Work
HNC(1-0)	516 ± 38	25	55 ± 11	1.28 ± 0.26	IRAM 30 m	Huettemeister et al. (1995)	...	55	14 ± 7	0.60 ± 0.30	SEST	Aalto et al. (2002)
	...	55	34 ± 7	0.79 ± 0.16	SEST	Aalto et al. (2002)						
	407	27.1	43 ± 8	0.96 ± 0.19	IRAM 30 m	Greve et al. (2009)						
	400	1.9 × 1.2	53 ± 5	1.4 ± 0.13	CARMA	2″, This Work	275	2.2 × 1.4	19 ± 4	0.89 ± 0.2	CARMA	2″, This Work
	425	0.7 × 0.5	58 ± 6	1.5 ± 0.15	CARMA	0.″8, This Work	275	0.8 × 0.5	18 ± 6	0.85 ± 0.3	CARMA	0.″8, This Work
HCO^+(1-0)	...	4.1 × 2.2	20 ± 6	0.48 ± 0.14	IRAM PdBI	Radford et al. (1991)	420	2.0 × 1.7	21 ± 3	0.93 ± 0.13	NMA	Nakanishi et al. (2005)
	...	...	19 ± 6	0.46 ± 0.14	IRAM 30 m	Solomon et al. (1992a)	...	28	25 ± 8	1.11 ± 0.35	IRAM 30 m	Graciá-Carpio et al. (2006)
	...	28	22 ± 7	0.53 ± 0.17	IRAM 30 m	Graciá-Carpio et al. (2006)						
	570	2.0 × 1.2	37 ± 4	1.0 ± 0.11	CARMA	2″, This Work	470	2.2 × 1.3	40 ± 4	2.0 ± 0.19	CARMA	2″, This Work
	450	0.7 × 0.5	36 ± 4	0.96 ± 0.1	CARMA	0.″8, This Work	470	0.7 × 0.6	48 ± 5	2.3 ± 0.2	CARMA	0.″8, This Work
^{13}CO(1-0)	369	22.4	9 ± 2	0.14 ± 0.03	IRAM 30 m	Greve et al. (2009)						

Table 1
(Continued)

Line	ARP 220						NGC 6240					
	FWHM (km s^{-1})	HPBW (arcsec)	$S_\nu\Delta v$ (Jy km s^{-1})	L'^c ($\times 10^9$ K km s^{-1} pc^2)	Telescope	References	FWHM (km s^{-1})	HPBW (arcsec)	$S_\nu\Delta v$ (Jy km s^{-1})	L'^c ($\times 10^9$ K km s^{-1} pc^2)	Telescope	References
	380	1.7 × 0.9	14 ± 2	0.24 ± 0.04	CARMA	2″, This Work	...	...	...	...	...	...
	300	0.5 × 0.4	11 ± 1	0.19 ± 0.02	CARMA	0.″8, This Work	...	...	...	...	...	...
$H^{13}CN$(1-0)	400	2.0 × 1.3	15 ± 2	0.43 ± 0.06	CARMA	2″, This Work	...	...	...	...	...	...
	380	0.7 × 0.5	17 ± 2	0.48 ± 0.05	CARMA	0.″8, This Work	...	0.7 × 0.6	7 ± 2	0.37 ± 0.1	CARMA	0.″8, This Work
^{13}CS(2-1)	...	...	...	...	...	...	...	...	...	...	...	...

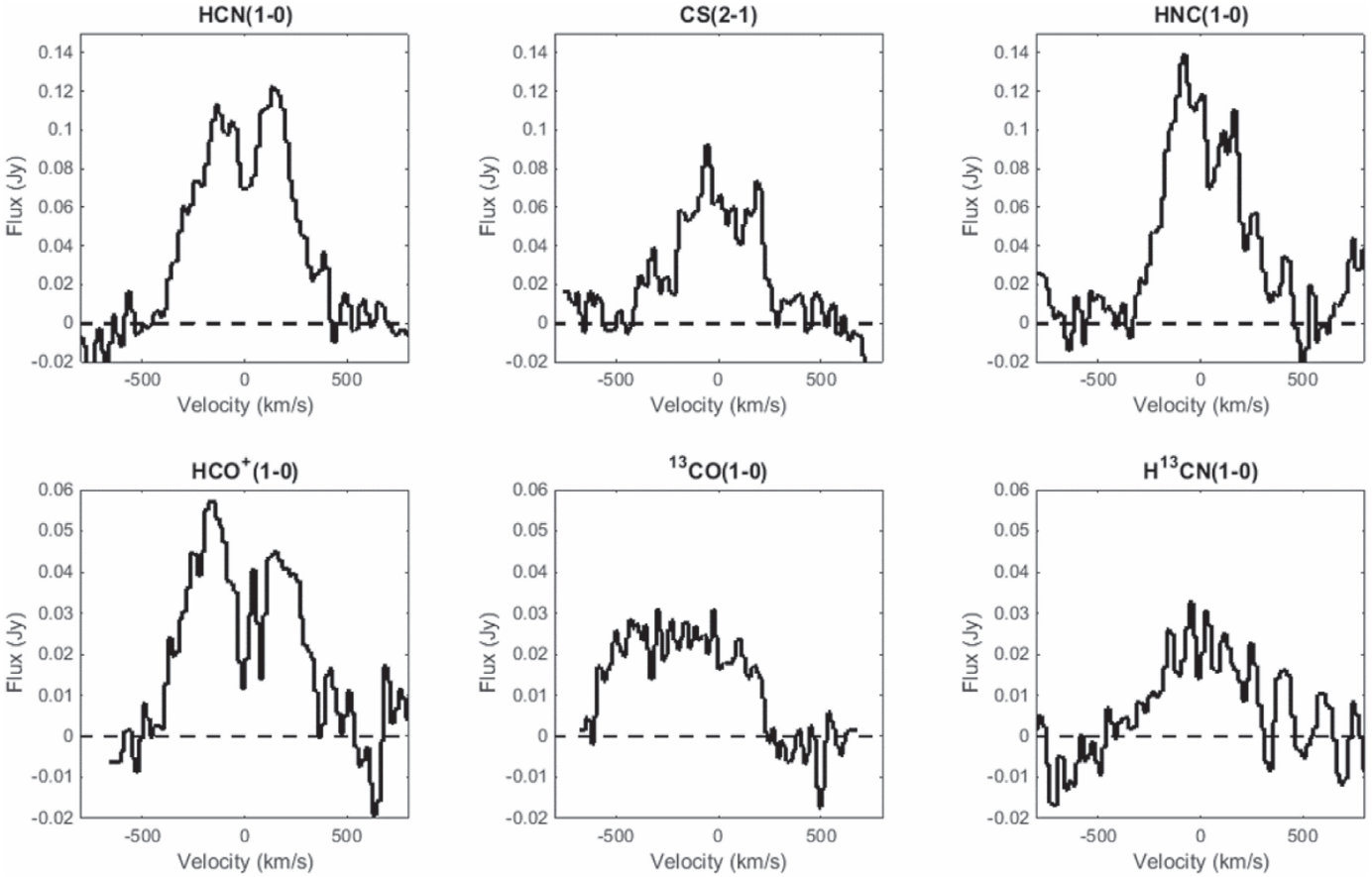

Figure 1. Molecular line spectra for Arp 220. The velocity scale for all transitions is the same and centered at the Galaxy redshift. The flux scale for HCN(1-0), CS(2-1), and HNC(1-0) transition spectra (panels (a)–(c)) are the same. The HCO^+(1-0), ^{13}CO(1-0), and $H^{13}CN$(1-0) spectra (panels (d)–(f)) scales are stretched to show the weaker spectra features.

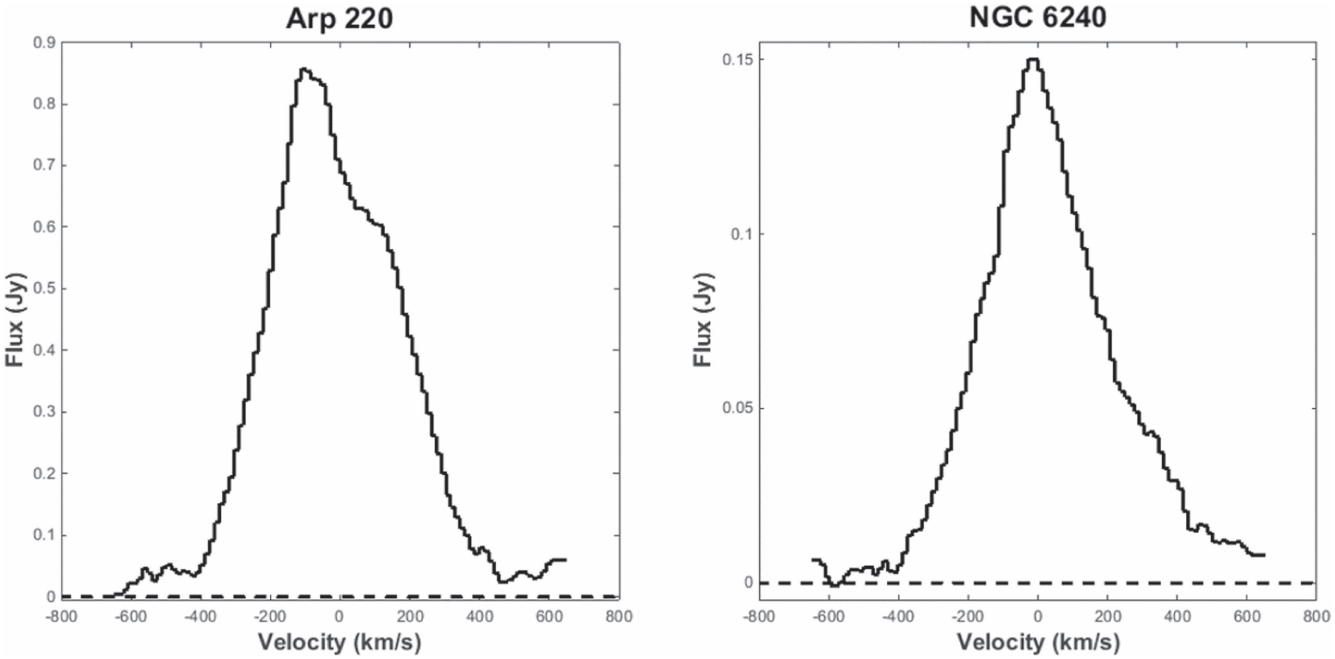

Figure 2. Molecular CO(1-0) spectra for Arp 220 and NGC 6240. The velocity scales are the same as those adopted in Figure 1 for Arp 220 and Figure 3 for NGC 6240. The velocity limits are the same for both the galaxies. In both galaxies the CO intensity is much greater than for the other lines. For NGC 6240, the scale adapted here is expanded by a factor of 6 compared to Figure 3.

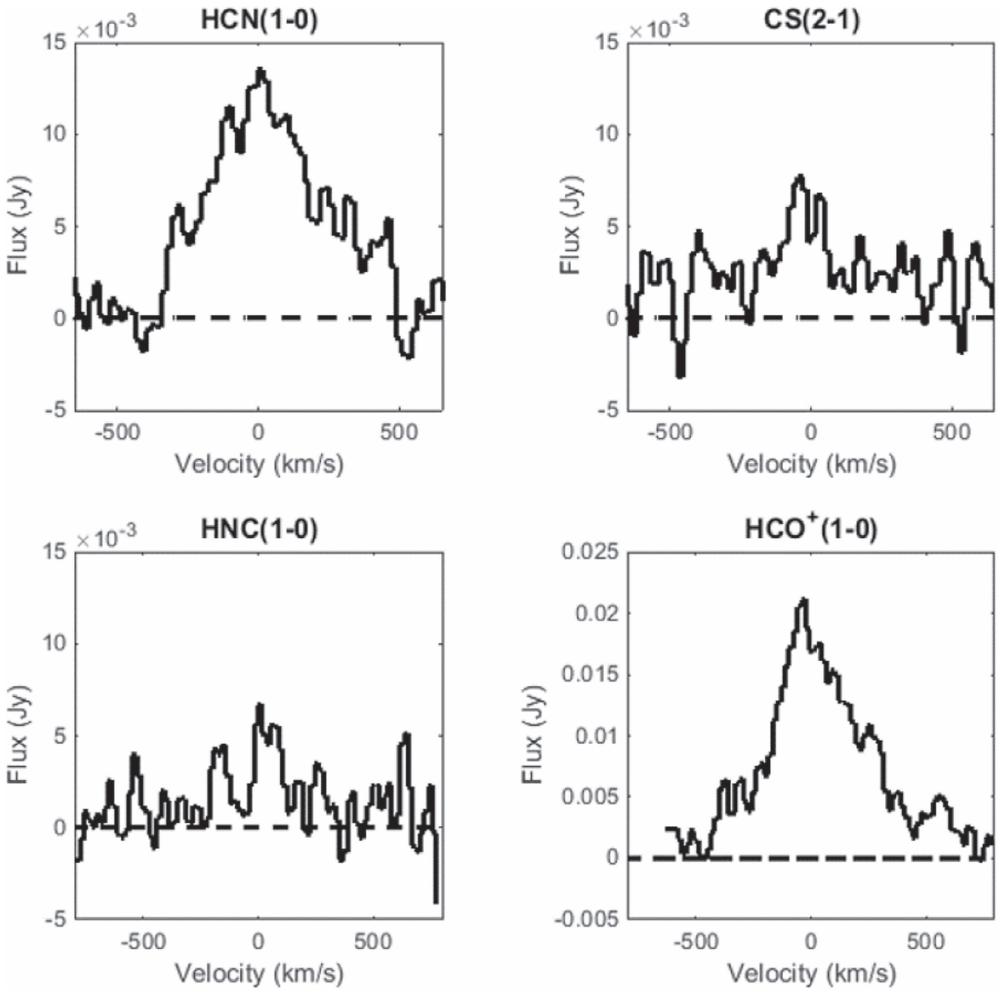

Figure 3. Molecular line spectra observed in NGC 6240. The velocity scale for all transitions is the same and centered at the Galaxy redshift. HCN(1-0), CS(2-1), and HNC(1-0) transition spectra (panels (a)–(c)) are on the same flux scale. The HCO^+(1-0) spectra has the highest peak of the transitions and its flux scale is higher. Note that the vertical scales in all panels except (d) have a scale factor of 10^{-3}.

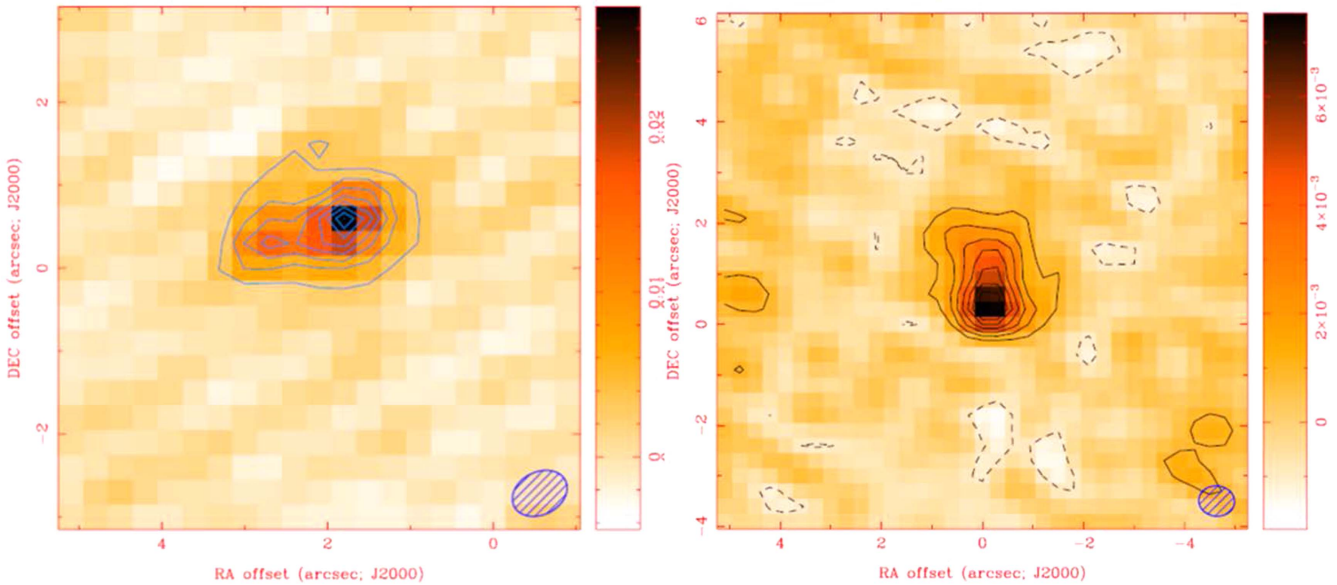

Figure 4. Arp 220 (left) and NGC 6240 (right) integrated line intensity images for HCN(1-0) emission at $0\farcs6$ resolution. Contours are at 2σ separations starting at 4σ. The beam size is shown in the lower right corner for both images.

Table 2
Constants Used for Large Velocity Gradient Modeling for Arp 220 and NGC 6240

Line	B (GHz)	A_{ul} (s^{-1})	Abundance, X Relative to H_2	Arp 220 T_b (K)	Arp 220 dv/dr (s^{-1})	NGC 6240 T_b (K)	NGC 6240 dv/dr (s^{-1})
HCN(1-0)	44.32	2.4×10^{-5}	2×10^{-8}	22.1	1.3×10^{-13}	15.2	3×10^{-14}
CS(2-1)	24.50	1.7×10^{-5}	5×10^{-9}	13.2	1×10^{-13}	8	1.5×10^{-14}
HNC(1-0)	45.33	2.7×10^{-5}	4×10^{-9}	22.8	1×10^{-13}	10.4	2.3×10^{-14}
HCO^+(1-0)	44.59	4.3×10^{-5}	4×10^{-8}	14.4	1.3×10^{-13}	19.1	4×10^{-14}

4. Analysis and Discussion

4.1. High Density Molecular Gas Traced in HCN, CS, HNC, and HCO^+

A major goal of this study was to measure various molecular tracers at matched resolution and with consistent calibration. This enables analysis of the relative line strengths to provide reliable molecular abundances and gas physical conditions.

For the molecular excitation analysis, we used the Large Velocity Gradient or Sobolev formalism to treat the radiative transfer and then solve for the molecular level populations assuming statistical equilibrium (Goldreich & Kwan 1974; Scoville & Solomon 1974). For the line photon escape probabilities we assume a spherical cloud geometry yielding $\beta = (1 - \exp^{-\tau})/\tau$, where τ is the line optical depth.

The molecular level populations are determined by detailed balance of collisional excitation and de-excitation by H_2 molecules, spontaneous decay in the permitted dipole transitions and absorption, and stimulated emission in optically thick molecular lines. The latter is termed "line photon trapping" and it effectively results in the spontaneous decay rates being reduced by the photon escape probability, i.e., the Einstein A coefficient is replaced by βA. This means that the critical densities of the transitions can be considerably reduced when the transitions become optically thick. Scoville et al. (2015) made use of a two-level analytic approximation for the excitation analysis for CS (7-6) and HCN (4-3) in Arp 220 and NGC 6240; here, we incorporate the full multi-level statistical equilibrium to yield more accurate results.

Simultaneous solutions for the multilevel non-LTE populations were obtained using the Newton–Raphson method with code made available by Jin Koda through private communication. The populations for each molecular species are a function of the gas volume density n_{H2}, the gas kinetic temperature T_k, the molecular abundance X_m relative to H_2, and the line of sight velocity gradient dv/dr. The collisional cross sections are from RADEX (Schöier et al. 2005). For the adopted kinetic temperature and dv/dr appropriate for each source, the excitation temperature, T_x and optical depth of each rotational transition can then be determined as a function of n_{H2} for an adopted molecular abundance. As a starting point, we used abundances for the different molecule similar to those of Galactic GMCs (see below). We then let those relative abundances vary in order that a consistent volume density n_{H2} is derived for each observed species—HCN, CS, HNC, and HCO^+. The parameters used for the LVG model are detailed in Table 2 for Arp 220 and NGC 6240.

Our observations constrain the peak *apparent* brightness temperature, T_b, for each of the transitions HCN(1-0), CS(2-1), HNC(1-0), and HCO^+(1-0) in both Arp 220 and NGC 6240. Assuming the lines are optically thick, these apparent brightness temperatures are 15–25 K for Arp 220 and 10–20 K for NGC 6240. The apparent brightness temperature is lower than the true brightness temperature due to beam dilution effects if the emission source does not entirely fill the synthesized beam. To compensate for this partial filling, we make use of the observed CO (1-0) *apparent* brightness temperature and assume that this emission has a similar beam filling factor as the high dipole moment molecules. Since the CO levels are more easily thermalized ($T_x = T_k$), the ratio of the observed T_b of each molecular line to that of CO provides an approximate estimate of the ratio of each molecular excitation temperature to the gas kinetic temperature T_k. We then try to match the molecular excitations with the observationally constrained T_x/T_k.

This analysis is implicitly assuming that CO and the higher dipole moment molecules have the same beam filling factor. If the other molecules have a smaller beam filling then their excitation temperatures could be larger than those given by the ratio of the brightness temperature and the CO brightness temperature.

The preceding methodology was used to estimate the gas density for each of the observed transitions in Arp 220 and NGC 6240. In the case of Arp 220 the observed emission nucleus is ~130 pc in diameter, and in NGC 6240 the diameter of our imaged disk is ~380 pc. Using the velocity FWHM of each transition in the respective galaxies, we obtained the values of dv/dr listed in Table 2. For both galactic nuclei, we adopt a mean kinetic temperature of ~45 K based on the dust temperature measured in IR spectral energy distributions (Sanders et al. 1991). We assume that the dust and gas are likely to be approximately in thermal equilibrium, as should be the case at densities $n_{H2} > 10^4\,cm^{-3}$ (Goldreich & Kwan 1974).

We also assumed the abundance of HCN relative to molecular hydrogen, H_2, to be similar to that seen in Galactic clouds, with $X_{HCN} \sim 2 \times 10^{-8}$ (Bergin et al. 1996; Lahuis & van Dishoeck 2000) where $n_m = X_{HCN} n_{H2}$. In the case of CS, the galactic abundance has been observed to be $X_{CS} \sim 5 \times 10^{-9}$ (Paglione et al. 1995; Shirley et al. 2003; Bergin et al. 1997).

For the HNC(1-0) transition, Graninger et al. (2014) postulate $X_{HNC} \sim X_{HCN}$. Therefore, we first adopted $X_{HNC} \sim 2 \times 10^{-8}$ for our calculations. However, this assumption resulted in values of n_{H2} that were too low compared with measurements made using other molecular species. We then adjusted the abundance of HNC to X_{HNC} to $\sim 4 \times 10^{-9}$, 5 times lower than previously assumed and redid our calculations. The adjusted abundances resulted in more comparable values of n_{H2}. The lower abundance of HNC in contrast to HCN could be due to the destruction of HNC molecules at higher temperatures. At gas densities $n(H_2) > 10^5\,cm^{-3}$, the HNC chemistry is dominated by reactions like

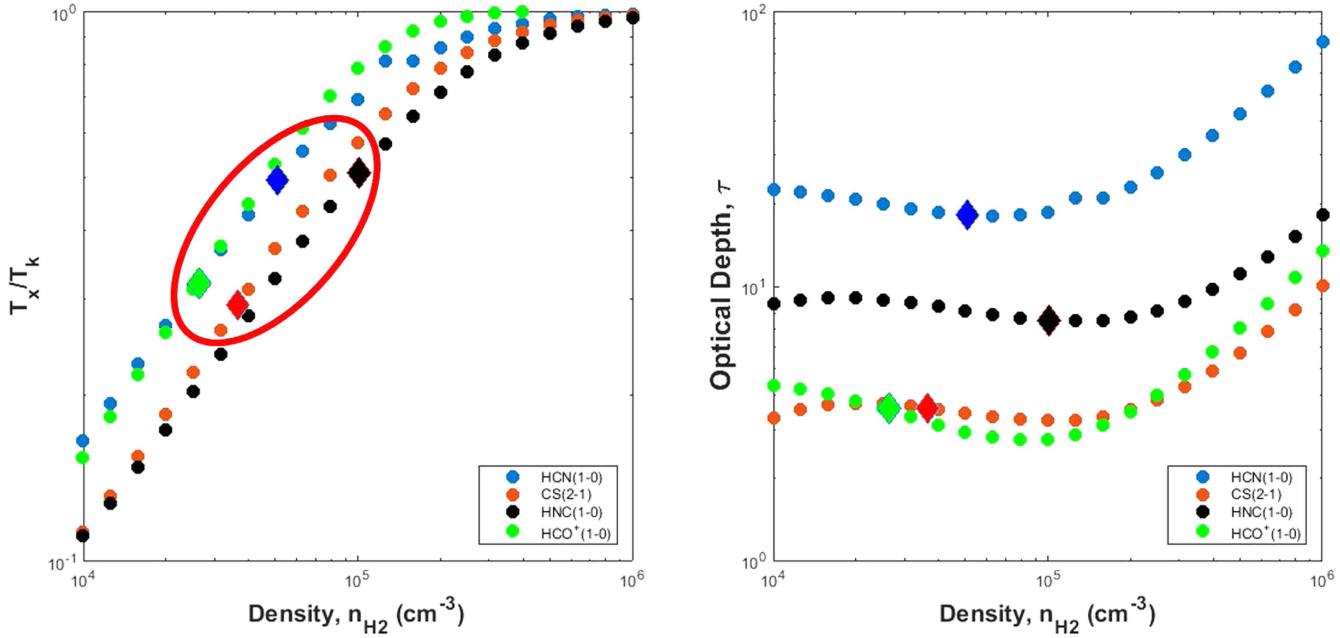

Figure 5. Arp 220: on the left, the ratio of the level excitation temperature to the gas kinetic temperature (T_x/T_k) on the abscissa and the density of HCN(1-0), CS(2-1), HNC(1-0), and HCO^+(1-0) lines. On the right, optical depths of each of the lines are shown.

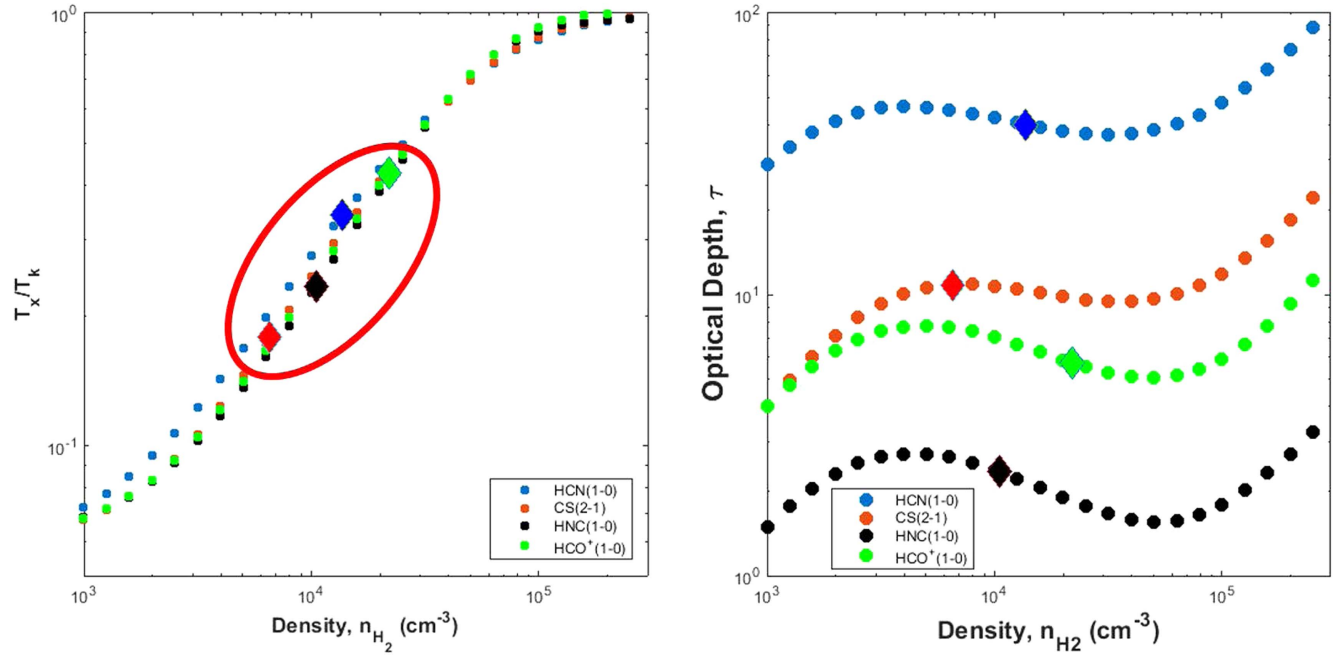

Figure 6. NGC 6240: on the left, the ratio of the level excitation temperature to the gas kinetic temperature (T_x/T_k) on the abscissa and the density of HCN(1-0), CS(2-1), HNC(1-0), and HCO^+(1-0) lines. On the right, optical depths of each of the lines are shown.

$HNC + O \longrightarrow CO + NH$ which would destroy HNC at higher temperatures (Goldsmith et al. 1981; Hirota et al. 1998).

Initially, we adopted an abundance of HCO^+ relative to molecular hydrogen, H_2, that was twice that of HCN (Acharyya & Herbst 2015). Hence, $X_{HCO^+} \sim 4 \times 10^{-8}$. With this assumption, the derived n_{H2}, yielding the observed ratio T_x/T_k, was an order of magnitude lower than expected from the excitation of the other molecular species. In order that the derived n_{H2} agree, the HCO^+ abundance was reduced to $X_{HCO^+} \sim 4 \times 10^{-9}$. In fact, the abundance of HCO^+ is expected to decline at higher gas volume densities due to increased recombination in denser regions. The required low abundance may simply reflect the fact that the density of the entire nuclear gas concentration is high, not unlike core regions enveloped in a lower density medium.

The left panels in Figures 5 and 6 show the ratio T_x/T_k calculated for all the transitions in Arp 220 and NGC 6240. The observed values of T_x/T_k measured for each transition are shown as diamond shaped points on the plots. For the adopted abundances in Arp 220, the required molecular hydrogen densities, n_{H2}, are $5 \times 10^4\,cm^{-3}$ for HCN, $4 \times 10^4\,cm^{-3}$ for CS, $1 \times 10^5\,cm^{-3}$ for HNC, and $3 \times 10^4\,cm^{-3}$ for HCO^+. For

the adopted abundances in NGC 6240, the required densities, n_{H2}, are $1 \times 10^4\,cm^{-3}$ for HCN, $7 \times 10^3\,cm^{-3}$ for CS, $1 \times 10^4\,cm^{-3}$ for HNC, and $2 \times 10^4\,cm^{-3}$ for HCO^+. We are assuming a single gas kinetic temperature as given by the IR color temperature (see above).

The right panels in Figures 5 and 6 show the line optical depth for each of the transitions as a function of density. The optical depths for the above mentioned densities are marked with diamond shaped points in the subplots. In the case of Arp 220, the optical depths, τ, are 20 for HCN, 4 for CS, 8 for HNC and 4 for HCO^+. For NGC 6240, the optical depth τ is 40 for HCN, 10 for CS, 3 for HNC and 6 for HCO^+. Thus, these lines are optically thick as assumed earlier for both galaxies. ^{13}CO intensity measurements did not fit the model used for the other lines and yielded optical depth, $\tau \approx 1$ and $n_{H2} \sim 10^2$. This may imply either that the $^{13}CO/CO$ abundance is much lower than the galactic abundances or that the ^{13}CO emission is originating from a clumpy medium.

In Arp 220, measurements and calculations for all species produced similar molecular gas densities for the assumed abundances. As already described, the assumed abundances of HNC and HCO^+ were adjusted to fit the molecular hydrogen densities. Since n_{H2} should be constant regardless of which molecular species was used to make the estimate, this suggests that the abundances in galactic sources may not apply to ULIRGs or each of the transitions traces a different area in the source.

In the case of NGC 6240, we adopted the abundances derived for Arp 220. All the transitions indicate molecular gas densities within a factor of 2 of these assumed abundances. As in the case of Arp 220, the values of n_{H2} calculated from HNC and HCO^+ measurements suggest a difference between abundances of these species in ULIRGs and galactic clouds.

4.1.1. Reduced Abundances of HNC and HCO^+ in ULIRGs

In summary, the consistent H_2 density is $5 \times 10^4\,cm^{-3}$ in Arp 220 and $10^4\,cm^{-3}$ in NGC 6240. This value was obtained for both the 2″ and 0.″5–0.″8 resolution observations. The initial abundances we adopted were typical of Galactic sources. However, in the case of HNC, this adopted abundance (Graninger et al. 2014) led to H_2 densities 5 times lower than those measured using HCN. For HCO^+, the assumed Galactic abundance (Acharyya & Herbst 2015), implied an H_2 density that is an order of magnitude lower than for HCN. These discrepancies imply that the HNC and HCO^+ abundances in the ULIRGs Arp 220 and NGC 6240 are very significantly reduced from what is implied for standard Galactic GMC cloud cores. The disagreement in the values is probably rooted in the physical conditions in the molecular gas in these galaxies. HNC is preferentially destroyed at higher temperatures than HCN, which would therefore result in lower abundances of HNC. HCO^+ abundances might be diminished as a result of recombination in very dense conditions.

The mean gas density in the nuclei of Arp 220 is 5 times higher than that in NGC 6240, although the dynamical masses of the galaxies are similar $\sim 5 \times 10^9\,M_\odot$ in the disk of NGC 6240 (Tacconi et al. 1999) and $2 \times 10^9\,M_\odot$ in each of the disks of Arp 220 (Scoville et al. 1997, 2015). The denser molecular gas in Arp 220 compared to NGC 6240 may reflect the fact that Arp 220 is very likely more advanced in the merging process and the gas is concentrated in the two nuclear disks rather than in the interaction zone between the nuclei as in NGC 6240.

4.2. HCN and HNC Line Ratios: XDR versus PDR Regions

The HCN and HNC abundance ratios provide constraints on the temperature, density, and environment of the molecular gas in galaxies. An important aspect is whether the region is photon dominated (PDR) or X-ray dominated (XDR). Differentiating between these is insightful; a PDR would imply that the molecular gas is mainly radiated by extreme star formation while an XDR would imply that the molecular gas is irradiated by an AGN. Since it is not always clear whether there is an obscured AGN in the core of a galaxy, this can provide important information about the nature of the luminosity source.

PDRs are characterized by the irradiation of molecular gas clouds in star-forming regions by far-ultraviolet (FUV) radiation emitted by young, nearby, OB type stars. O and B stars dominate the radiation from starbursts, which is mostly in the FUV, $6.0 < E < 13.6$ eV (Tielens & Hollenbach 1985). Since a starburst galaxy will be populated by a large number of OB stars, it is expected that the molecular gas in such regions will be dominated by PDR chemistry. FUV photons dominate the ionization and spectral properties, and physical conditions such as temperature and densities, especially on the surface of the molecular clouds. The fraction of the dense molecular gas dominated by PDR conditions is in general small since the dust extinction in the molecular gas is generally high. However, in a nuclear starburst the young stars may be more uniformly distributed throughout the dense gas, hence producing a larger fraction of dense gas in the PDR condition.

XDRs are characterized by the irradiation of molecular gas clouds by intense X-ray fluxes. Molecular gas can be irradiated by X-rays in a number of different astrophysical scenarios, e.g., near AGNs, supernovae remnants, and X-ray binaries. The dominant source of X-rays in ULIRGs such as Arp 220 and NGC 6240, which may have supermassive accreting black holes, would be AGNs. These are capable of producing hard X-ray photons with energies >1 keV, which can penetrate through large column densities, $\sim 10^{22}\,cm^{-2}$, before being absorbed by the molecular gas because of the large energy per photon present in the radiation (Maloney et al. 1996). This can strongly alter the chemical and thermal properties of clouds that are opaque to other kinds of radiation.

The effects of X-ray irradiation can also result in infrared and submillimeter emission from the irradiated molecular clouds. By observing these effects, the presence of an XDR (indicating perhaps the existence of an obscured AGN) can be deduced. Many investigations into the properties of XDRs have been carried out over the years (Krolik & Kallman 1983; Lepp & McCray 1983; Bakes & Tielens 1994; Maloney et al. 1996). Recent studies (Meijerink & Spaans 2005; Meijerink et al. 2007), employ updated models, including a vast range of densities and temperatures, to predict the properties of emission lines of molecular species such as HCO^+, HCN, HNC, and CS. These models and our new emission line observations enable us to probe the molecular gas environment and the nature of the energy source both Arp 220 and NGC 6240.

X-ray observations of both Arp 220 and NGC 6240 have suggested the presence of AGNs. Since both galaxies are merging systems, it appears that they both have supermassive black holes (SMBHs). While these systems are at different merging states, they have not gone through the coalescing stage, which would include the merger of the black holes at

their cores. In Arp 220, we clearly observe two counter-rotating disks of gas, both of which probably have black holes at their centers. The presence of at least one black hole has been indicated from X-ray observations (Clements et al. 2002; McDowell et al. 2003); the other has yet to be detected. In the case of NGC 6240, the two black holes have been detected (Komossa et al. 2003) using *Chandra X-Ray Observatory*.

Using the molecular emission line measurements, we might be able to detect the presence of SMBHs in the midst of the molecular gas if the molecular clouds are being irradiated under XDR conditions. Given the very high column densities of dust, the absence of the optical emission line ratios characteristic of AGNs does not preclude the presence of a SMBH. Line ratio measurements for the molecular species consistent with the XDR models would be a very strong indicator of its presence.

The densities of molecular gas that we are probing using high density gas tracers like HCN, HNC, and CS are expected to be of the order of 10^4–$10^6\,\mathrm{cm}^{-3}$. HCN and HNC molecules have very similar critical densities because of their similar dipole moments. Therefore, the line ratios should be strong indicators of their abundance and the environment of the molecular gas. The models of XDRs indicate that the HCN/HNC column density ratio is diminished (and lower than unity) compared to PDRs and quiescent cloud regions for gas densities around $10^5\,\mathrm{cm}^{-3}$. Steady-state excitation models show that the abundance of HCN and its isotopomer HNC decreases with increasing density and temperature (Schilke et al. 1992). Values for the HCN/HNC abundance ratio above unity are consistent with steady-state models for higher-density gas at higher temperatures (Meijerink et al. 2007). An HNC/HCN abundance ratio lower than unity suggests a rather quiescent, low temperature gas.

At higher temperatures, HNC tends to be selectively destroyed in favor of HCN as long as the medium is not highly ionized. Therefore, HCN/HNC is roughly unity in PDR sources, but lower than unity in XDR sources. The HNC/HCN abundance ratio is expected to be around 0.9 if the standard neutral production paths are followed (Goldsmith et al. 1981). In a highly ionized medium, high HCN/HNC ratios would be prevented since $HCNH^+$ can form HCN and HNC with equal probability (Aalto et al. 2002; Wang et al. 2004). Shocks can selectively destroy HNC and could significantly increase the steady-state HCN/HNC abundance ratio (Schilke et al. 1992). Both HCN and HNC may also be pumped by an intense mid-IR radiation field boosting the emission from low density regions where the lines would not be collisionally excited. For HNC the interaction with the IR radiation is even stronger than for HCN, thus increasing the likelihood for IR pumping in extreme IR galaxies.

Table 3 displays the HCN/HNC line intensity ratios for the 1–0 transition for Arp 220 and NGC 6240 compiled using values from other sources such as Seyferts, Liners and Galactic Molecular Clouds (GMCs) for comparison. The uncertainty in the line ratios for our measurements is based on the uncertainty in our basic flux observations.

The dichotomy in the measurements for Arp 220 and NGC 6240 can be clearly seen. While the HCN/HNC ratio is less than unity for Arp 220, that is not the case for NGC 6240. The ratio for Arp 220 is clearly less than unity. As discussed earlier, a ratio less than unity indicates the presence of a strongly irradiated XDR, possibly by an AGN, at the cores of Arp 220. Since HNC(1-0) is a strong line in both nuclei as compared to HCN(1-0), there is a clear indication that both may house an AGN irradiating the molecular gas.

Table 3
HCN and HNC Line Ratios for Arp 220 and NGC 6240

Galaxy	$\frac{\mathrm{HCN(1–0)}}{\mathrm{HNC(1–0)}}$	Reference
NGC 3079	2.15 ± 0.67	Pérez-Beaupuits et al. (2007)
NGC 1068	2.01 ± 0.65	Pérez-Beaupuits et al. (2007)
NGC 2623	1.4	Aalto et al. (2002)
NGC 1365	1.35 ± 0.37	Pérez-Beaupuits et al. (2007)
NGC 7469	1.50 ± 0.57	Pérez-Beaupuits et al. (2007)
L1489	0.83 ± 0.17	Hirota et al. (1998)
L1521B	0.5 ± 0.12	Hirota et al. (1998)
ARP 220	0.79 ± 0.1	This Work
NGC 6240	1.39 ± 0.2	This Work

In contrast, NGC 6240, where two AGNs have been detected in other observations, displays a line ratio higher than unity. Such a ratio is expected from molecular gas with PDR conditions. That is not to say that a XDR does not exist within the galaxy but certainly indicates that the molecular gas clouds we are observing have been mostly been irradiated by radiation originating from star forming regions. The ratio observed in NGC 6240 is very similar to other known star-forming galaxies as shown in Table 3. This is consistent with the fact that the molecular gas peak lies between the two nuclei and not on top of them.

In summary, the diminished HCN/HNC ratio in both nuclei of Arp 220 may indicate the presence of an XDR being associated with an AGN. NGC 6240 does not show a diminished HCN/HNC ratio, despite confirmed AGN detections, presumably because the molecular gas lies between the two nuclei and is not irradiated by the AGN.

5. Summary

We present a unique set of observations where we observed the high density gas tracers HCN, CS, HNC, and HCO^+ along with CO and their isotopomers at high resolution and high sensitivity in Arp 220 and NGC 6240. Such an interferometric data set provides an excellent probe into the dense molecular gas cores of these galaxies wherein lie the answers to many questions about star formation and the correlation between starbursts, AGN activity, and merging. We used CARMA to image these galaxies at 2″ and 0.″5–0.″8 resolutions.

Using the Large Velocity Gradient formalism, we derived the molecular hydrogen densities and optical depth at measured brightness temperatures for each of the molecular species. The H_2 densities were of the order of $5 \times 10^4\,\mathrm{cm}^{-3}$ for the assumed abundances for each of the molecular species in Arp 220, and $10^4\,\mathrm{cm}^{-3}$ in NGC 6240. The abundances we assumed were taken from observations of Galactic sources. Initially, in the case of HNC, calculations using these assumed abundances (Graninger et al. 2014) resulted in H_2 densities 5 times lower than those measured using HCN. In the case of HCO^+, the assumed abundance (Acharyya & Herbst 2015) gave H_2 densities an order of magnitude lower than HCN.

This discrepancy leads us to suggest that the abundances we measure for HNC and HCO^+ in our Galaxy do not hold for ULIRGs such as Arp 220 and NGC 6240. The disagreement in the values is probably rooted in the physical conditions in the

molecular gas in these galaxies. HNC is preferentially destroyed at higher temperatures in comparison to HCN, and therefore would result in lower abundances of HNC. HCO^+ abundances might be diminished as a result of recombination in very dense conditions. In fact, the abundances of these molecular species could be as much 10 times different from Milky-Way-like galaxies.

Understanding the chemistry of HCN and HNC molecules has allowed theorists to model their behavior in XDR versus PDR regions in galaxies. These models predict a HCN/HNC ratio of less than 1 in XDR conditions in the molecular gas. We find the ratio in Arp 220 to be significantly less than unity. Arp 220 does not have confirmed X-ray detections of AGNs in either nucleus. Our measurement of the HCN and HNC ratio in Arp 220, at both resolutions, strongly indicates an XDR, which is probably being irradiated by an AGN. For the first time, both Arp 220 nuclei show AGN signatures.

In contrast, we did not get indications of an XDR in NGC 6240, which does have two X-ray confirmed AGNs. The majority of the nuclear gas lies between the two AGNs in NGC 6240 and is presumably not as irradiated by the AGN. Therefore, the molecular gas does not show XDR conditions in the molecular gas but shows PDR conditions. This indicates that the molecular gas in merging systems goes through phases of XDR and PDR conditions as the merger takes place, and this changes the abundances in the merging systems with time.

We thank our referee for the thorough report which has helped improve the paper. We gratefully acknowledge the assistance of Anneila Sargent for suggestions and improvements on the manuscript. We thank the staff of CARMA for their help with carrying out the observations and calibrations. We thank Marc W. Pound and Peter Teuben for their invaluable help with data reduction. CARMA development and operations were supported by the National Science Foundation grants AST-0838260 and AST-1140063 under a cooperative agreement, and by the CARMA partner universities. We acknowledge student support from NRAO under grants AST-0956545 and AST-0836064. We thank Jin Koda for lending us the LVG modeling code.

References

Aalto, S., Booth, R. S., Black, J. H., & Johansson, L. E. B. 1995, A&A, 300, 369
Aalto, S., Polatidis, A. G., Hüttemeister, S., & Curran, S. J. 2002, A&A, 381, 783
Acharyya, K., & Herbst, E. 2015, ApJ, 812, 142
Anantharamaiah, K. R., Viallefond, F., Mohan, N. R., Goss, W. M., & Zhao, J. H. 2000, ApJ, 537, 613
Bakes, E. L. O., & Tielens, A. G. G. M. 1994, ApJ, 427, 822
Bayet, E., Aladro, R., Martín, S., Viti, S., & Martín-Pintado, J. 2009, ApJ, 707, 126
Bergin, E. A., Goldsmith, P. F., Snell, R. L., & Langer, W. D. 1997, ApJ, 482, 285
Bergin, E. A., Snell, R. L., & Goldsmith, P. F. 1996, ApJ, 460, 343
Beswick, R. J., Pedlar, A., Mundell, C. G., & Gallimore, J. F. 2001, MNRAS, 325, 151
Bryant, P. M., & Scoville, N. Z. 1999, AJ, 117, 2632
Clements, D. L., McDowell, J. C., Shaked, S., et al. 2002, ApJ, 581, 974
Downes, D., & Eckart, A. 2007, A&A, 468, L57
Downes, D., & Solomon, P. M. 1998, ApJ, 507, 615
Engel, H., Davies, R. I., Genzel, R., et al. 2010, A&A, 524, A56
Goldreich, P., & Kwan, J. 1974, ApJ, 189, 441
Goldsmith, P. F., Langer, W. D., Ellder, J., Kollberg, E., & Irvine, W. 1981, ApJ, 249, 524
Graciá-Carpio, J., García-Burillo, S., Planesas, P., & Colina, L. 2006, ApJL, 640, L135
Graninger, D. M., Herbst, E., Öberg, K. I., & Vasyunin, A. I. 2014, ApJ, 787, 74
Greve, T. R., Papadopoulos, P. P., Gao, Y., & Radford, S. J. E. 2009, ApJ, 692, 1432
Hirota, T., Yamamoto, S., Mikami, H., & Ohishi, M. 1998, ApJ, 503, 717
Huettemeister, S., Henkel, C., Mauersberger, R., et al. 1995, A&A, 295, 571
Iwasawa, K., Sanders, D. B., Evans, A. S., et al. 2005, MNRAS, 357, 565
Komossa, S., Burwitz, V., Hasinger, G., et al. 2003, ApJL, 582, L15
Krips, M., Neri, R., García-Burillo, S., et al. 2008, ApJ, 677, 262
Krolik, J. H., & Kallman, T. R. 1983, ApJ, 267, 610
Lahuis, F., & van Dishoeck, E. F. 2000, A&A, 355, 699
Lepp, S., & McCray, R. 1983, ApJ, 269, 560
Maloney, P. R., Hollenbach, D. J., & Tielens, A. G. G. M. 1996, ApJ, 466, 561
McDowell, J. C., Clements, D. L., Lamb, S. A., et al. 2003, ApJ, 591, 154
Meijerink, R., & Spaans, M. 2005, A&A, 436, 397
Meijerink, R., Spaans, M., & Israel, F. P. 2007, A&A, 461, 793
Nakanishi, K., Okumura, S. K., Kohno, K., Kawabe, R., & Nakagawa, T. 2005, PASJ, 57, 575
Paglione, T. A. D., Jackson, J. M., Ishizuki, S., & Rieu, N.-Q. 1995, AJ, 109, 1716
Papadopoulos, P. P., Zhang, Z.-Y., Xilouris, E. M., et al. 2014, ApJ, 788, 153
Pérez-Beaupuits, J. P., Aalto, S., & Gerebro, H. 2007, A&A, 476, 177
Radford, S. J. E., Delannoy, J., Downes, D., et al. 1991, in IAU Symp. 146, Dynamics of Galaxies and Their Molecular Cloud Distributions, ed. F. Combes & F. Casoli (Cambridge: Cambridge Univ. Press), 303
Sakamoto, K., Scoville, N. Z., Yun, M. S., et al. 1999, ApJ, 514, 68
Sanders, D. B., Mazzarella, J. M., Kim, D.-C., Surace, J. A., & Soifer, B. T. 2003, AJ, 126, 1607
Sanders, D. B., Scoville, N. Z., & Soifer, B. T. 1991, ApJ, 370, 158
Sanders, D. B., Soifer, B. T., Elias, J. H., et al. 1988, ApJ, 325, 74
Schilke, P., Walmsley, C. M., Pineau Des Forets, G., et al. 1992, A&A, 256, 595
Schöier, F. L., van der Tak, F. F. S., van Dishoeck, E. F., & Black, J. H. 2005, A&A, 432, 369
Scoville, N., Sheth, K., Walter, F., et al. 2015, ApJ, 800, 70
Scoville, N. Z., Evans, A. S., Thompson, R., et al. 2000, AJ, 119, 991
Scoville, N. Z., Sargent, A. I., Sanders, D. B., & Soifer, B. T. 1991, ApJL, 366, L5
Scoville, N. Z., & Solomon, P. M. 1974, ApJL, 187, L67
Scoville, N. Z., Yun, M. S., & Bryant, P. M. 1997, ApJ, 484, 702
Shirley, Y. L., Evans, N. J., II, Young, K. E., Knez, C., & Jaffe, D. T. 2003, ApJS, 149, 375
Solomon, P. M., Downes, D., & Radford, S. J. E. 1992a, ApJL, 387, L55
Solomon, P. M., Downes, D., & Radford, S. J. E. 1992b, ApJL, 398, L29
Solomon, P. M., Downes, D., Radford, S. J. E., & Barrett, J. W. 1997, ApJ, 478, 144
Tacconi, L. J., Genzel, R., Tecza, M., et al. 1999, ApJ, 524, 732
Tielens, A. G. G. M., & Hollenbach, D. 1985, ApJ, 291, 722
Veilleux, S., Kim, D.-C., & Sanders, D. B. 2002, ApJS, 143, 315
Wang, M., Henkel, C., Chin, Y.-N., et al. 2004, A&A, 422, 883